



Size-dependent cyclic voltammetry study of silicon microwire anodes for lithium ion batteries



Sandra Hansen^{a,*}, Enrique Quiroga-González^b, Jürgen Carstensen^a, Helmut Föll^a

^a Institute for Materials Science, Kiel University, 24143 Kiel, Germany

^b Institute of Physics, Benemérita Universidad Autónoma de Puebla (BUAP), 72570 Puebla, Mexico

ARTICLE INFO

Article history:

Received 25 May 2016

Received in revised form 19 August 2016

Accepted 18 September 2016

Available online 19 September 2016

Keywords:

Li-ion battery

Si wires

pre-lithiated silicon

cyclic voltammetry

battery potential

ABSTRACT

Silicon microwires as anodes for Li-ion batteries may show good cycling performance over 100 cycles as anodes for Lithium ion batteries without significant capacity losses. The life time of the anode, however, strongly depends on the way the battery is charged. Overcharging or undercharging may have severe negative consequences. This paper studies with the study of the operational voltage range of Si microwire anodes and its dependence on the dimensions of the wires. Cyclic voltammetry is used to identify the potentials for the different lithiation/delithiation events, while a modified cyclic voltammetry technique is used to study the dynamics of those processes. Specially prepared anodes with Si wires of different lengths and widths were used for the study.

© 2016 Published by Elsevier Ltd.

1. Introduction

Graphite is the most commonly used anode material for Li ion batteries due to its low cost and large cycle life, although it presents low capacities of around 370 mAh/g [1,2]. Nevertheless, this capacity is not enough to satisfy the demands for higher capacity of several applications. Besides being able to store large amounts of charge, the anode has to withstand many cycles without being damaged. Silicon, offering the highest gravimetric capacity for anode materials, of 4200 mAh/g pulverizes when used in bulk state due to volume expansions during cycling. However, if it is micro-/nano-structured, it can withstand large volume changes during lithiation/delithiation [3–5]. In particular, Si microwire array anodes with wires of 1 μm in diameter have shown exceptionally good performance [6,7]. To achieve this performance, it is important to charge the batteries in the correct potential range.

Charging outside the proper operating range of the battery produces large leakage currents that may lead to temperature increase inside the battery, producing electrolyte decomposition or an explosion of the battery in the worst case [1,8]. On the other hand, Li-ion batteries in general suffer from memory effects, which occur when a battery is charged within its voltage limits but in a smaller voltage range. The system remembers the smaller limits

and for the next charging cycles it can only be charged to these limits [1], decreasing the usable capacity. All these factors affect the life time of a battery. Therefore, it is important to find the correct potential limits of the Si microwire anode.

It can be deduced from different reports of electrode materials that the lithiation and delithiation voltages depend on the size and geometry of the anode itself [9–13]. For example, for Si wires thinner than 100 nm, the potential of fully lithiated wires is in the range of 50 mV to 70 mV vs. Li/Li⁺ [9–12]. On the other hand, if the wires are thicker than 100 nm, a shift to higher potentials has been observed [11]. Up to now, no research has fully clarified how the dimensions of the electrodes affect the lithiation/delithiation potentials. In order to determine if variations of the size of the Si microwires induce a voltage shift in the lithiation or delithiation process, the diameter as well as the length of the wires have been varied in this work, and have been tested by cyclic voltammetry. To reduce the resistances outside the wires and to minimize process differences (e.g. during deposition of the current collector), they have been tested in a paste electrode configuration, with a large amount of conductive carbon. Compared to the highly-ordered array anodes without any additives, paste electrodes as used in this study show a ten times lower capacity when cycled under same conditions. However, the objective of the work is not to present top performing anodes, but to study some phenomena occurring in Si wires using cyclic voltammetry. This technique is the method of choice in this paper to estimate the size dependency. Additionally, the current relaxation in the anode is studied with a special

* Corresponding author. Tel.: +49 431 880 6180; fax: +49 431 880 6124.

E-mail addresses: sn@tf.uni-kiel.de (S. Hansen), equiroga@ieee.org (E. Quiroga-González), jc@tf.uni-kiel.de (J. Carstensen), hf@tf.uni-kiel.de (H. Föll).

voltammetry method to determine the lithiation/delithiation kinetics in relation to the size of the wires.

2. Experimental Details

The preparation of the Si microwires consists of a two-step process starting with a pre-structured (100) p-type Si wafer with a resistivity of 15–25 Ωcm . The finished, pre-structured pattern on the wafer is a quadratic array of inverted quadratic pyramids, with a pitch of 3 μm ; for details about pre-structuring see [3,14]. The first step of the fabrication process is the electrochemical etching of macropores (Fig. 1 a–c). Fig. 1 shows a schematic of the process to produce Si microwires, step by step, beginning with pre-structuring of Si substrates.

The pores grow at the pits of the pyramids due to sharp tips increasing the probability of nucleation at those points, as described by the current burst model (see Fig. 1c–d) [15]. The process is temperature controlled at 18 °C. The mixed aqueous and organic electrolyte allows to control the pore diameter modulation as well as the pore wall passivation, which is necessary to fine control the wire thickness of the wires. By adjusting the current density during electrochemical etching and due to the addition of PEG into the electrolyte, the pores can be modulated [3,16]. The etching current profile was optimized to get a homogeneous pore diameter along the length of the pores. Depending on the current profile, different pore lengths (translated in different wire lengths at the end of the process) can be obtained. The second step is a chemical over-etching process of the pore walls in an aqueous low concentrated KOH-based solution at 50 °C (Fig. 1e). After this process the Si microwires are obtained. Depending on the etching time, wires with different thicknesses can be prepared.

For the voltammetric studies two sets of Si microwires were produced: a) wires 60 μm long with thicknesses of 1.8 μm , 1.6 μm , 1.4 μm , 1.2 μm ; b) wires 1.4 μm thick with lengths of 75 μm , 60 μm , 46 μm , 36 μm .

Examples of the produced wires with different thicknesses and lengths are shown in the SEM images in Fig. 2.

Fig. 2a and b show wire arrays with two different thicknesses of 1.4 and 1.6 μm at a fixed length of 60 μm . In the figure, the wires

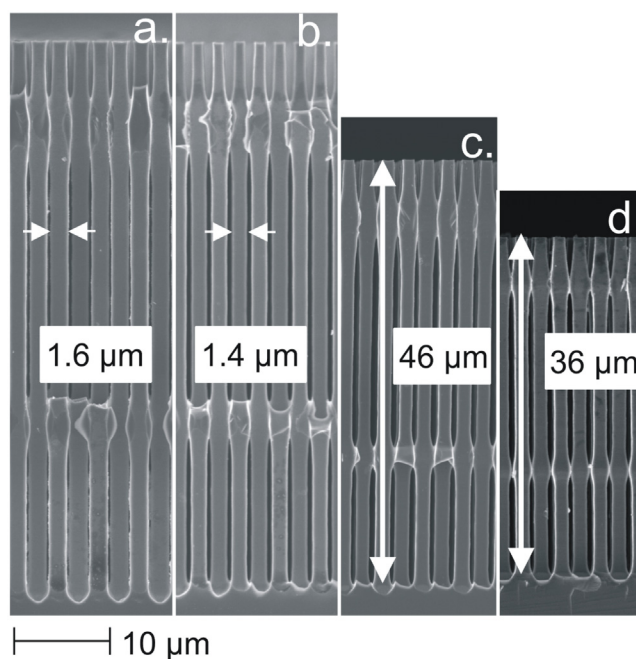


Fig. 2. Examples of wires with different thickness and length: Wires of a. and b. have the same length of around 60 μm , and widths of 1.6 and 1.4 μm , respectively. The wires of c. and d. have the same thickness of 1.4 μm , but different lengths of 46 and 36 μm , respectively.

are still attached to the Si substrate. The wires show two diameter modulations which are used as diffusional barrier and to stabilize the diameter. Fig. 2c and d show wires with different lengths, but with the same thickness, in order to systematically investigate the influence of the thickness and the length of the Si microwires on the peak potentials and with it on the voltage limits during cycling experiments. With this electrochemical etching method, highly reproducible and reliable anodes were produced, by step-by-step adapting thickness or length of the wires.

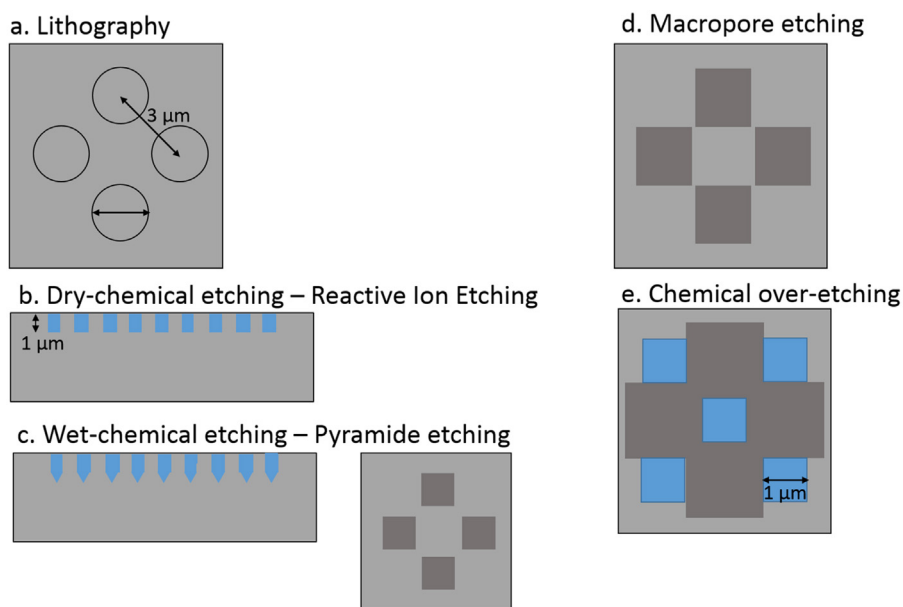


Fig. 1. Schematic of the fabrication steps of the Si microwires. a. It shows the pre-structuring via lithography with a highly ordered pattern. b. and c. It includes the dry and wet chemical pre-structuring process which are a requirement for the essential macropore etching step. The essential macropore step is shown in d in a top view. During the over-etching step, the interstices between the pores is dissolved and the wires remain free-standing.

Battery cycling experiments with Si microwire anodes connected to a copper plate indicate a good cycling stability but experience noticeable ohmic losses along the wires [7,17]. Paste electrodes are used in this study to avoid the series resistance limitations and ohmic losses, allowing to test the intrinsic properties of the wires inside the anodes. The paste electrodes consist of an equal amount of Si microwires (active material) and carbon black (CB, conducting agent) in a proportion 45 wt.%: 45 wt.%. Fig. 3a and b show SEM images and the corresponding EDX analysis for the paste electrodes containing Si microwires. The images show how the wires are embedded and contacted with the CB particles which form a high percolating network around the wires.

Although the amount of the carbon is rather high, the carbon is electrochemically inert. The carbon in this paste is not lithiating or taking up Li^+ -ions. Its only function is to enhance the conductivity of the paste and reduce the ohmic losses. In order to exclude that the CB takes part in the reaction between the Li ion and the Si microwires, anodes without Si microwires (only CB and binder are present) are tested as reference, as seen in Fig. 4b. The cyclic voltammety measurements showed no phase transformations between CB and the Li atoms, indicating a “normal” charging behavior of a capacitor (see Fig. 4b). The results were compared to those ones with only binder (not shown here). They show all the same results, with small differences given by the dielectric constant of the material between plates.

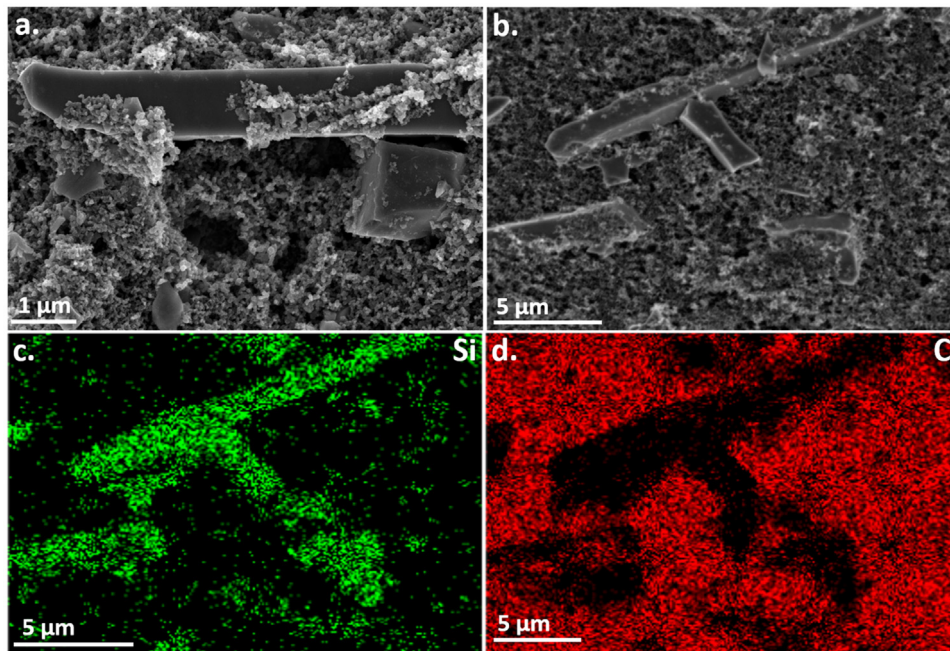


Fig. 3. SEM and EDX analysis of Si Paste anodes. a. – b. The SEM images show how the Si microwires are embedded and surrounded by the spherical carbon black particles. c. – d. Corresponding EDX maps showing the components of the paste, silicon and carbon (sodium from the cellulose is negligible).

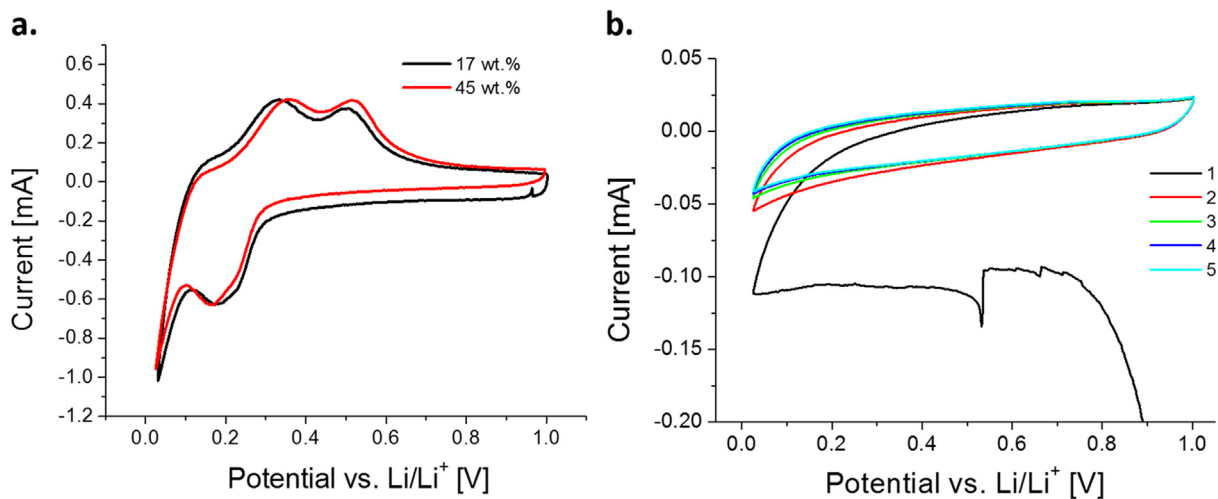


Fig. 4. a. Voltammograms of paste anodes with different concentrations of carbon black. The adhesion to the current collector is enhanced and the segregation within the paste is limited when increasing the amount of carbon black particles. b. Voltammograms of electrodes without Si microwires (with only CB and CMC). The curve resembles the behavior of a capacitor.

Impedance spectroscopy data show that the only function of the carbon black is to enhance the conductivity and to facilitate the binding between CMC and silicon [18–22]. High amounts of carbon black as conducting agents should enhance the conductivity of the percolating network around and between the silicon wires. Furthermore, the high amount reduces the extend of volume expansion during lithiation. Reducing the carbon black to only 17 wt.% (Fig. 4a), the mixing and electrochemical properties change. High amounts of conductive additives have the advantage to form a percolating network around the silicon wires without losing the contact to the silicon during volume expansion, and enable the possibility that all of the silicon wires are contacted to the current collector. In samples with lower amounts of CB the electric contact to the Si microwires could be lost. It is clear that commercial electrodes maximize the amount of active material, minimizing the amounts of conductive additives and binders to reduce weight. The purpose of the test electrodes fabricated in this work is specifically the characterization of the active material and not of the electrode performance [19].

The remaining 10 wt.% is of sodium carboxymethylcellulose (CMC), which was used as binder. As Obrovac et al. and Cerbelaut et al. stated, the right choice of binder material could not only influence the battery performance but also affect the interaction between the active material and the conductive carbon [19–22]. The binder in paste electrodes has a large influence on the electrochemical diffusion and kinetics. Additional Fast-Fourier-Transform Impedance Spectroscopy measurements (not shown here, published elsewhere) indicated that the type of binder influences the segregation of the paste during lithiation and delithiation, possibly hindering the kinetics inside the paste. Once the wires are embedded in the paste with CMC around them, they expand during lithiation, shifting the conducting material. Upon delithiation, the silicon material shrinks back, moving CB back. This depends on the elastic constant of the binder material. The cellulose needs more time to reconnect to the active material, leaving behind non-connected material which superimpose diffusional losses on the system. The advantage of CMC, as in the case of this study, is that it chemically binds on the silicon surface in form of bridges or springs [21,23–27]. It can accommodate stresses during lithiation/delithiation better than other binders. Without the chemical adsorption to silicon, as is the case of PVDF [23,28], it comes to a complete segregation inside the paste. This is also caused by the change in elastic properties of that type of binder upon cycling.

Si microwires, CB, and CMC were mixed with water droplets in a mortar to enable a homogeneous mixture. The paste was then coated on a Cu current collector. Fig. 3 shows an example of the paste anode produced. As can be seen in Fig. 3, the carbon black is contacted equally from the sides to the Si microwires. On the top of the wires, small fibres, known as the CMC material, can be seen.

Prior to assembly in an Ar filled glove box, the anodes were dried at 85 °C for 10 h under vacuum. The Si anodes were tested in half cells with electrolyte LP 30 (11.80 wt.% LiPF₆ in ethylene carbonate and dimethyl carbonate (1:1), BASF) and glass fiber separators of Whatman, with a pore size of 1.5 μm and a thickness of 1305 μm. A Li metal foil with a thickness of around 2 mm was used as counter and reference electrode.

The voltammetry measurements were performed with a potentiostat from ET & TE GmbH. All the measurements were performed at room temperature. These experiments were done over five cycles with a voltage sweep rate of 0.1 mVs⁻¹ in the voltage range from 1 V to 0.02 V to prevent lithium plating (see the voltammogram of Fig. 6). The inset in the voltammogram shows a typical potentiostatic profile where the typical scan is shown between the voltage limits.

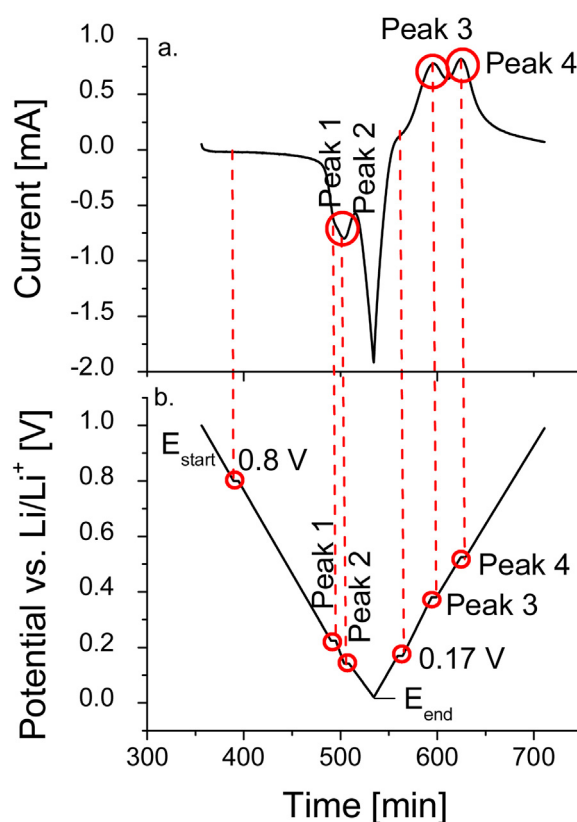


Fig. 5. Profile for the modified cyclic voltammogram for studying relaxation processes. a. The figure shows the constant steps at the peak positions and at two additional positions where no peaks are present. E_{start} and E_{end} indicate the starting and end potential of the scans, respectively. For reference, the length of the constant voltage steps is 5 min., b. The figure shows a typical current-time profile where the peaks indicate phase transformations. The dashed lines indicate where the constant steps are applied.

Additionally, to get information about the lithiation/delithiation time constants, a modified cyclic voltammetry profile was used. For these experiments, the parameters like voltage range as well as the sweep rate of 0.1 mVs⁻¹ remained the same. The slow sweep rate was chosen to establish an electrochemical equilibrium between the active species. Increasing the sweep rate would increase the displacement current (current caused by a double layer capacitor charging) making the identification of the peaks attributed to phase transformations much more difficult. Fig. 5 shows the applied potential with the modified constant voltage steps. Above that applied potential, a typical current-time profile of a voltammogram is shown. The dashed lines indicate where the constant steps were initiated/applied (correlation to the voltammogram). The time for the constant steps is relatively short to minimize changes in the state of charge (SOC), but long enough to appreciate the shape of the current decay (here 5 minutes, see Fig. 5). Experiments showed that longer constant steps shift the SOC too much, influencing the peak potentials. If the voltage is held constant for longer times, the SOC of the battery dramatically changes and the voltammetric peaks can be shifted. As indicated in Fig. 5 with red circles, besides keeping the potential constant at the four peak positions, it was also kept constant at 0.8 V during the reverse scan and at 0.170 V during the forward scan. The two additional steps are applied to differentiate between the charge transport mechanisms at the potentials of the peaks (see Fig. 5), and the capacitive charging effects in forward and reverse voltage sweeps. A typical result of such a modified step voltammogram could be seen in Fig. 11. The aim of this kind of experiments is the

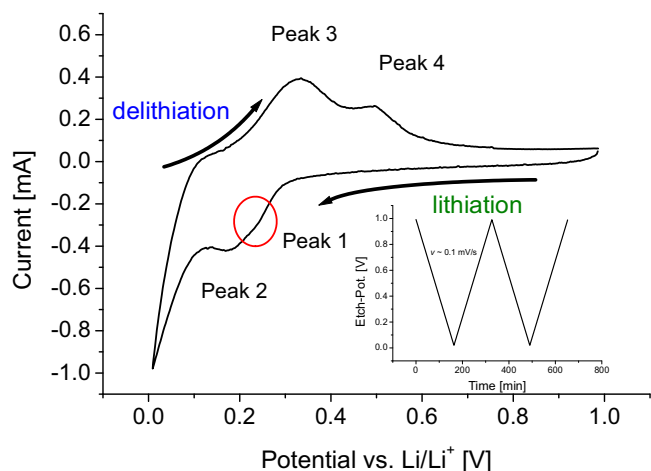


Fig. 6. Typical cyclic voltammogram of the Si microwires in half cells. The system is fully reversible at a slow voltage sweep rate.

analysis of the diffusional behavior of the Li^+ -ions when incorporating into the Si anode. In contrast to “normal” voltammetric measurements, modified “step” voltammetry enables the possibility to distinguish the relaxation times, also depending on the geometry.

3. Results and Discussion

Cyclic voltammetry is a potentiostatic method commonly used to analyze the charging/discharging mechanisms of electrodes for Li-ion batteries [29–31]. The peaks occurring during these measurements represent (possible) phase transformations, redox reactions with the electrodes, or, as in the case of the present study, formation of alloys of Li with the electrode components [29,30]. A typical cyclic voltammogram obtained by analyzing the samples of the present study is shown in Fig. 6. It shows four peaks; two lithiation and two delithiation peaks at different potentials. The inset in the figure shows the applied potential scan. As discussed above, the voltage sweep rate is slow to allow recording peak potential changes. The incorporation of Li^+ -ions is a fully reversible two-step process. When the measurement starts, the (crystalline) Si anode contains no lithium, which gets incorporated with the ongoing measurement.

The first lithiation peak (Peak 1) represents the partial lithiation of Si leading to amorphous $\text{Li}_{13}\text{Si}_4$ alloys [6,10,11]. Further lithiation (going to reduced potentials) leads to the fully lithiated phase $\text{Li}_{22}\text{Si}_5$, represented by Peak 2 [11], (although there is a bit controversy about the real composition of this phase). Obrovac et al. reported that this fully lithiated phase has the composition of $\text{Li}_{15}\text{Si}_4$ [5,10], but the investigations of other authors confirm the existence of $\text{Li}_{22}\text{Si}_5$ [11,32]. In fact, for wires of around $1\ \mu\text{m}$ in diameter, as is the range of the wires of the present work, the formation of $\text{Li}_{22}\text{Si}_5$ was shown by XRD [6].

For the delithiation, the reverse process occurs. First the incorporated Li^+ -ions are partially removed to the Li_xSi_y phase (Peak 3) [6,10,11] and then fully delithiated Si is obtained (Peak 4) [11].

3.1. Potentials for lithiation and delithiation

Fig. 7 shows the peak positions obtained by cyclic voltammetry for the lithiation and delithiation (cycle number 3) for different wire lengths, versus Li. The potentials can be translated into voltage drops ΔV , that are the differences between the potential of the peaks and the initial potential for the voltage sweep. For the

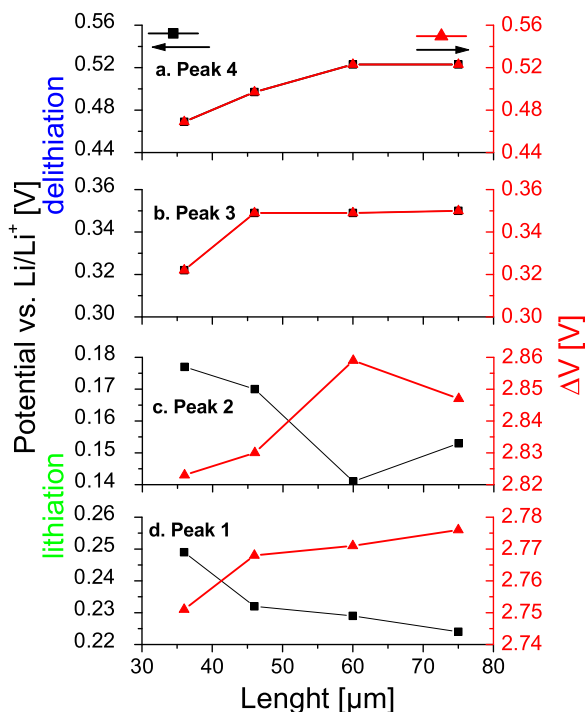


Fig. 7. Peak potential vs. wire length. The solid line is a guide for the eyes. a. Peak 4, b. Peak 3, c. Peak 2, d. Peak 1.

lithiation process, ΔV can be calculated as $\Delta V = \text{open circuit potential (3 V for the present anodes)} - \text{potential of the peak}$. For the delithiation process it can be approximated to $\Delta V = \text{potential of the peak} - \text{reference potential (0 V, Li)}$. These voltages are shown on the right Y-axis in the plots of Fig. 7.

By comparing the potentials for the two lithiation peaks (Fig. 7c and d, square symbols), both curves show a similar tendency. Both potentials decrease when the wires are longer. The peak position shifts to smaller values. On the other hand, for the delithiation peaks, the tendency is opposite (see Fig. 7a and b). The peak position shifts to higher values as the wires become longer. Taking the values of ΔV for all the peaks (triangle shaped curves, right Y-axis) into account, it is clear that they all increase for longer wires, independently of the process (lithiation or delithiation). According to this, it can be said that the voltage needed for the incorporation or removal of Li^+ -ions inside the Si wires is larger for longer wires.

The increase in ΔV when increasing the length of the wires can be explained with a series resistance model. The schematic in Fig. 8 shows an example of the effect of the series resistances, considering wires of two different lengths. The schematic shows how the wires are contacted to the copper current collector. The wires are embedded in a conducting matrix. The total electric resistance of the wires can be seen as a series of resistances R_n . The value of the resistances of two wires is the same if their dimensions are exactly the same. If the thickness of the wires is exactly the same, but their length varies, it is easy to understand that the wires have more or less R_n elements in series (see Fig. 8). However, Li^+ -ions may move through the solid – electrolyte interface and into the anode from all sides, as depicted in Fig. 8. According to this, the resistance for the electron transfer in the different paths could be larger or smaller than the nominal resistance given by the dimensions; even though, the average resistance R_{ave} is directly proportional to the length of the wires. As an example, Fig. 8 shows wires Wire 1 and Wire 2 with lengths L_1 and L_2 , respectively. The depicted case is the simplest, where the current collector (carbon black) is at one end of the wires. However, the model is similar if

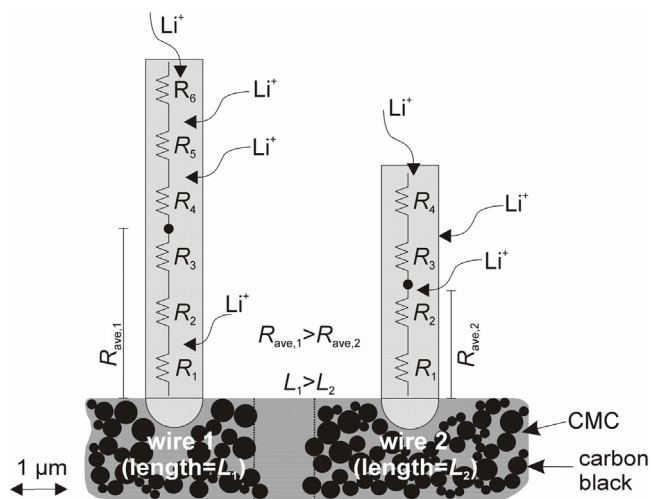


Fig. 8. Series resistance of wires with different lengths L_1 and L_2 . Li^+ -ions are incorporated from all directions, thus the Li^+ -ions encounter different resistances depending on their path, but the average resistance is R_{ave} . Also here the dashed line indicates separate samples.

the current collector is in a different position; in any case, L is the average length to the current collector. In Fig. 8, $L_1 > L_2$, since the number of resistors in series is larger in Wire 1 than in Wire 2. Consequently, R_{ave} in Wire 1 is larger. The increase in ΔV of Fig. 7 with the increment in length corresponds to an increase in resistance. The average resistance for shorter wires is smaller than for longer wires.

Fig. 8 shows the peak positions for the lithiation and delithiation for different wire thicknesses. The standard potential of Li^+ -ions is taken as reference. The trend of the lithiation peak positions is inverse to the trend observed with the length variation (see Fig. 9c and d, curve of square symbols). The potentials for the partial lithiation have smaller values for thicker wires, whereas the potentials for the fully lithiation peak have higher values. On the other hand, both delithiation peaks, in Fig. 9a and b, square shaped

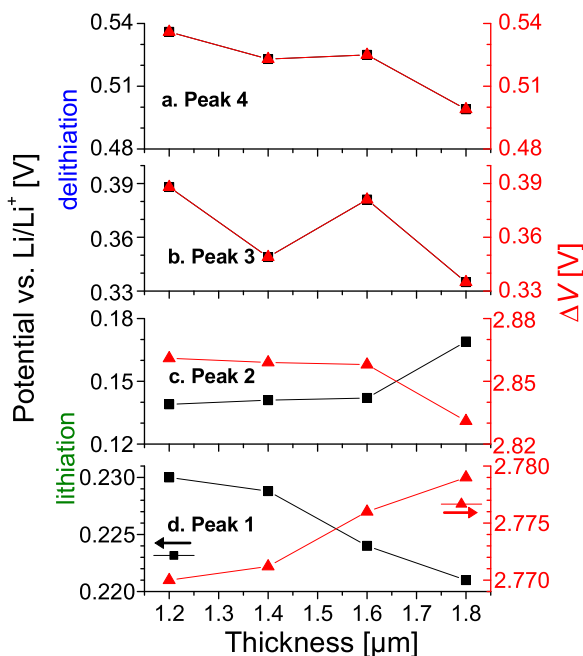


Fig. 9. Peak potential dependency on thickness. The solid line is a guide for the eyes. a. Peak 4, b. Peak 3, c. Peak 2, d. Peak 1.

dots, show the same tendency. The peak positions for the delithiation decrease for thicker wires. In Fig. 8 the potentials are also translated into voltage drops ΔV (right Y-axis), as in the case of length variation, represented by the curves of triangular shaped dots. Obviously, the thicker wires need more voltage for the first incorporation of Li^+ -ions (see Fig. 9d, triangular shaped curve) for the transformation of pure crystalline Si to partially lithiated Si. Once the Li^+ -ions are incorporated into the anode, the transformation to the fully lithiated state does not require a higher voltage in thicker wires, and ΔV even decreases (see Fig. 9c). In the case of delithiation, the ΔV values all decrease for thicker wires (see Fig. 9a and b). For the full lithiation and both delithiation peaks, the peak positions and the ΔV values show the same tendency. This implies that the incorporation and removal of Li^+ -ions in and from the anode is easier in thicker wires (less voltage is needed), with exception of the first lithiation event (Peak 1).

The decrease in ΔV for thicker wires can also be explained by a series resistance model. Fig. 9 shows exemplarily two wires with different thicknesses W_1 and W_2 . Here R'_n labels the resistance of the thicker wires. Obviously, $R_n > R'_n$ reflects that the resistance is inversely proportional to the size of the cross section. Similarly to the case of length variation, the Li^+ -ions can follow different paths with different resistances, but the average resistance varies with varying cross section. This translates into $R_{\text{ave},1} > R_{\text{ave},2}$ in Figs. 9 and 10. The reason for the decrease in potential in thicker wires (see Fig. 9) lies in the lower resistances in thicker wires, since ΔV is direct proportional to the resistance.

Quite astonishingly, the tendency of ΔV is reversed for the first lithiation peak, which implies that there should be a second phenomenon, but with opposite effect, also contributing to ΔV . This second contribution may be associated with the energy barrier for the first incorporation of Li^+ -ions. To overcome this barrier, Si-Si bonds have to be broken and Li^+ -ions have to diffuse into the Si matrix [13,33]. The covalent bonds between Si atoms are stronger than those between Si and Li atoms [13,33,34]. More energy has to be provided to disturb the Si network. Once the Si bonds are broken and the first Si-Li alloys are formed, it is easier to incorporate more Li^+ -ions.

Furthermore, the height of the potential barrier for the partial lithiation increases with increasing the surface area. This tendency could be explained by diffusion-induced stress. The activation energy for diffusion is highly dependent on the internal stresses. If tensile or compressive stress are present in the sample, the activation energy barrier is decreased or increased.

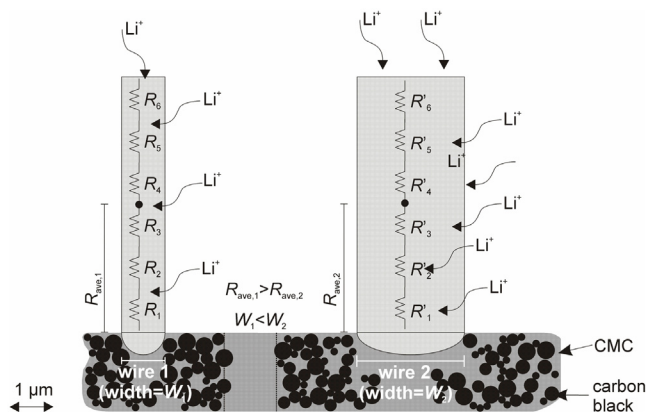


Fig. 10. Series resistance of wires of different thicknesses W_1 and W_2 . Li^+ is incorporated from all directions, thus the Li^+ -ions encounter different resistances depending on their path, but the average resistance is R_{ave} . Because the wires have the same length but a different thickness, their resistances are labeled R and R'_n . The dashed lines between the particles indicate that the wires are on separate samples.

The activation energy is an important factor for radial diffusion:

$$D = D_0 \exp(-\Delta E_b/RT) = D_0 \exp(-\alpha \Omega \sigma_b/RT) \quad (1)$$

where E_b is the stress-influenced activation energy, Ω the molar volume, D_0 the diffusion coefficient without internal stress [35], and σ_b is considered in cylindrical or spherical particles as circumferential and axial stresses whereas in planar particles it is considered as biaxial stress. The stress in cylindrical particles is proportional to the inverse square of the wire radius [35].

If the internal stress becomes larger in the case of a larger diameter of the wires, the activation energy and the diffusion are limited [35]. In this state, more atoms migrate and accumulate at the surface, leading to higher (compressive) stress. Thus more energy is needed to overcome the stress and to enable the (atomic) diffusion. When lithiating Si, there is a phase transition from pure crystalline Si to Li_xSi_y [36] producing larger compressive stress. This stress decreases the diffusion of Li^+ ions by increasing the energy barrier. After partial lithiation (Peak 1), the stress is released into tensile stress and the activation energy is reduced [35,36]. This suggests why the full lithiation event and the delithiation process of the wires seem to be unaffected by stress, and their potentials decrease as expected from the series resistance model.

The effect of compressive stress is only notorious in the voltammograms when changing the thickness of the wires. For wires with different lengths, the width of the wires is the same. The activation energy for those wires is relatively the same. Even though, in all cases presented here the energy for lithiation/delithiation is the sum of two contributions: it consists of the activation energy for each Li_xSi_y phase and the ohmic losses.

3.2. Relaxation times for lithiation/delithiation

To improve the understanding of the size dependency of the lithiation process, a special voltammetric technique consisting of a combination of cyclic voltammetry with stepwise voltammetry is applied. Stepwise scans have the advantage that they reduce the non-faradaic current contributions of the system [29,37,38]. Non-faradaic currents include the charging of the double layer capacitor formed between the battery electrodes, and shunt currents (direct electric paths between electrodes). They increase the amplitude of the voltammetric peaks (given by the faradaic processes), and they may shift their potentials. Faradaic currents, on the other hand, include the flow of electrons which leads to electrode reactions. These two currents have different time constants. The non-faradaic current associated to double layer capacitors exponentially decays to zero very fast and is negligibly small at the end of a constant voltage step [29,37]. To keep the influence of the non-faradaic currents small in cyclic voltammetry, it is always necessary to work with low voltage sweep rates. Only then the unwanted current contributions are negligibly small and the current output is mainly coming from the chemical reactions at the electrodes. The ratio between the faradaic and non-faradaic currents is then high.

Measurements with constant steps allow the determination of relaxation times, because the system tends to shift back to equilibrium. The relaxation time τ describes the diffusion of ions and is directly proportional to the resistance R through the relation $\tau = R * C$ (2). In this case C is not the electrical capacitance, but is related to the storage of charges electrochemically.

Fig. 11 illustrates an example of the resulting voltammogram when using the voltage profile of Fig. 5. As can be observed, the current decays at all four voltammetric peaks, and at the two additional steps at 0.8 and 0.17 V. A fit of the current decay at the first delithiation peak is shown in the inset.

At 0.8 V during the reverse scan, the current decreases linearly. At 0.17 V during the forward scan, the current decays exponentially

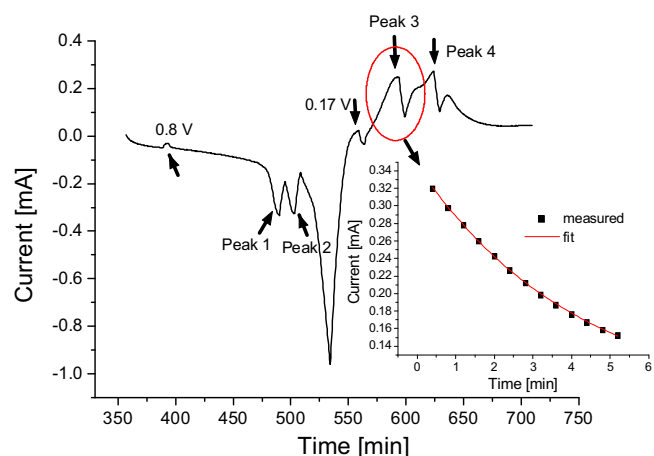


Fig. 11. Example of the modified step voltammogram and an example for the exponential fit for Peak 3 (inset).

but with a fast relaxation time constant of around 1 min. At these steps no electrode reaction is taking place and therefore the current is mainly non-faradaic.

During the constant steps at the peak positions, the current is decaying exponentially but with a slower relaxation time. The decaying current i can be fitted with an exponential curve given by the equation $i = i_0 + A \exp(-t/\tau)$ (3), where τ is the relaxation time, i_0 is a current offset, A is the intensity of the faradaic current at time 0, and t is the time. The same exponential fit can be used in all cases. The current at the voltammetric peaks is mostly faradaic which is built up due to reactions at the electrodes. Fig. 11 shows the comparison of the relaxation times of all four peaks which are orders of magnitude larger than those at 0.17 V, for wires of different length. The relaxation time increases for all peaks for longer wires. A larger value of the relaxation time for longer wires means a slower relaxation mechanism. From the cyclic voltammetry measurements it is known that the resistance is higher for long wires. According to equation (2), the larger the resistance, the larger the relaxation time.

The relationship between the conductivity of a wire and the diffusion can be explained/correlated with the Nernst-Einstein equation [39]. According to that, a lower conductivity is in direct connection to a small diffusion coefficient. The diffusion in longer wires takes more time than in shorter wires. The ionic transport in and out of the anode is hindered. The curves in Fig. 12 shift therefore to larger time values when the wires are longer.

The modified step voltammetry was also performed varying the thickness of the wires (see Fig. 13). The relaxation time for the lithiation and delithiation peaks decreases almost linearly with the thickness of the wires. This means that the relaxation time in thicker wires is faster than in thinner wires. The lithiation gets faster and easier as the thickness of the wires increases.

The relaxation time is faster in thicker wires due to their smaller resistance. On the other hand, considering the Nernst-Einstein model [39], it is easy to infer that as the conductance of thicker wires increases, the diffusion of Li^+ ions into and from the wires is faster.

4. Conclusion

In this paper the dependency of the lithiation and delithiation process on the different sizes of the Si microwires was proven. It was shown that there is a big difference in the peak development when analyzing thicker and longer wires. The thickness variation indicates that thicker wires show enhanced electronic and ionic

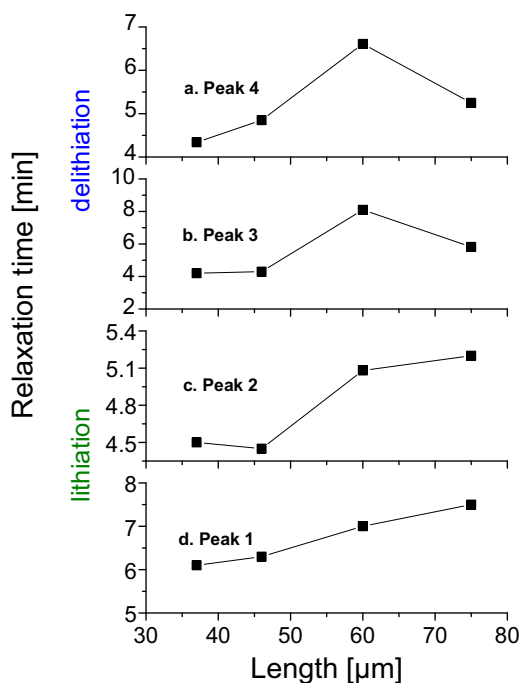


Fig. 12. Relaxation time dependency on the wire length. The solid line is a guide for the eyes. a. Peak 4, b. Peak 3, c. Peak 2, d. Peak 1.

conduction due to a smaller resistivity and a faster relaxation time. It has to be considered that it is necessary to overcome an energy barrier to start lithiating, which gets larger in thicker wires.

In addition to that, shorter wires show smaller resistivities and faster relaxation times. According to this, the incorporation of ions in the wires is easier when the wires are shorter.

The minimum voltage observed in the Si microwires of the present study ranges from 0.12 V to 0.082 V. In order to extend the

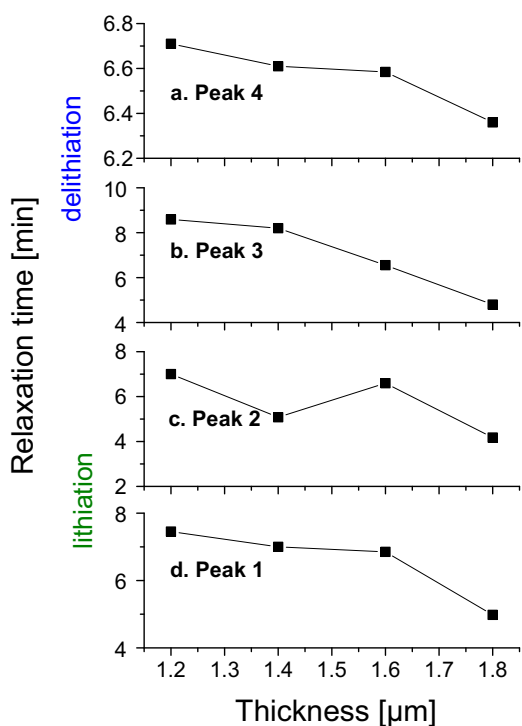


Fig. 13. Relaxation time dependency on the wire thickness. The solid line is a guide for the eyes. a. Peak 4, b. Peak 3, c. Peak 2, d. Peak 1.

life time of the Si microwire anodes in Li^+ -ion batteries, they have to be charged according to the dimensions of the wires.

Acknowledgements

Special thanks goes to the DFG for funding of this project “Elektrochemische und mikrostrukturelle Untersuchung der Prozesse in Anoden für Hochkapazitäts-Lithium-Ionen-Batterien basierend auf Si-Mikrodrahtanordnungen” (Fkz: FO 258/17-1). We kindly acknowledge Fabian Schütt for providing the EDX analysis.

References

- [1] A. Jossen, W. Weydanz, *Moderne Akkumulatoren richtig einsetzen*, Reichardt Verlag, Leipzig, 2006.
- [2] J.M. Tarascon, M. Armand, Issues and challenges facing rechargeable lithium batteries, *Nature* 414 (2001) 359.
- [3] E. Quiroga-Gonzalez, E. Ossei-Wusu, J. Carstensen, H. Föll, How to make optimized arrays of Si nanowires suitable as superior anode for Li-ion batteries, *J. Electrochem. Soc.* 158 (11) (2011) E119, doi:http://dx.doi.org/10.1149/1.3654197.
- [4] Y.M. Lin, K.C. Klavetter, P.R. Abel, N.C. Davy, J.L. Snider, A. Heller, C.B. Mullins, High performance silicon nanoparticle anode in fluoroethylene carbonate-based electrolyte for Li-ion batteries, *Chem. Commun.* 48 (2012) 7268, doi:http://dx.doi.org/10.1039/C2CC31712E.
- [5] J.J. Wu, W.R. Bennett, Fundamental Investigation of Si Anode in Li-Ion Cells, *NASA Energytech*, IEEE 5 (2012), doi:http://dx.doi.org/10.1109/energytech.2012.6304667.
- [6] E. Quiroga-Gonzalez, J. Carstensen, H. Föll, Structural and electrochemical investigation during the first charging cycles of silicon microwire array anodes for high capacity Lithium ion batteries, *Materials* 6 (2013) 626, doi:http://dx.doi.org/10.3390/ma6020626.
- [7] E. Quiroga-Gonzalez, J. Carstensen, H. Föll, Good cycling performance of high-density arrays of Si microwires as anodes for Li ion batteries, *Electrochim. Acta* 101 (2013) 93, doi:http://dx.doi.org/10.1016/j.electacta.2012.10.154.
- [8] T.B. Reddy, D. Linden, *Linden's handbook of batteries*, Mc Graw-Hill, New York (2011).
- [9] Y. Kubota, M.C.S. Escano, H. Nakanishi, H. Kasai, Crystal and electronic structure of $\text{Li}_{15}\text{Si}_4$, *J. Appl. Phys.* 102 (2007) 0537041, doi:http://dx.doi.org/10.1063/1.2775999.
- [10] M.N. Obrovac, L.J. Krause, Reversible Cycling of Crystalline Silicon Powder, *J. Electrochem. Soc.* 154 (2) (2007) A103, doi:http://dx.doi.org/10.1149/1.2402112.
- [11] K. Kang, H.S. Lee, D.W. Han, G.S. Kim, D. Lee, G. Lee, Y.M. Kang, M.H. Jo, Maximum Li storage in Si nanowires for the high capacity three dimensional Li-ion battery, *Appl. Phys. Lett.* 96 (2010) 0531101, doi:http://dx.doi.org/10.1063/1.3299006.
- [12] T.D. Hatchard, J.R. Dahn, In Situ XRD and Electrochemical Study of the Reaction of Lithium with Amorphous Silicon, *J. Electrochem. Soc.* 151 (6) (2004) A838, doi:http://dx.doi.org/10.1149/1.1739217.
- [13] V.L. Chevrier, H.M. Dahn, J.R. Dahn, Activation Energies of Crystallization Events in Electrochemically Lithiated Silicon, *J. Electrochem. Soc.* 158 (11) (2011) A1207, doi:http://dx.doi.org/10.1149/2.009111jes.
- [14] H. Föll, J. Carstensen, E. Ossei-Wusu, A. Cojocar, E. Quiroga-González, G. Neumann, Optimized Cu contacted Si nanowire anodes for Li ion batteries made in a production near process, *J. Electrochem. Soc.* 158 (5) (2011) A580, doi:http://dx.doi.org/10.1149/1.3561661.
- [15] J. Carstensen, M. Christophersen, G. Hasse, H. Föll, Parameter dependence of pore formation in silicon within a model of local current bursts, *Phys. Status Solidi A* 182 (1) (2000) 63.
- [16] E. Ossei-Wusu, J. Carstensen, E. Quiroga-González, M. Amirmaleki, H. Föll, The role of Polyethylene Glycol in Pore Diameter Modulation in Depth in p-type Silicon, *ECS J. Solid State Sci. Technol.* 2 (6) (2013) P243, doi:http://dx.doi.org/10.1149/2.020305jss.
- [17] E. Quiroga-Gonzalez, J. Carstensen, H. Föll, Optimal conditions for fast charging and long cycling stability of silicon microwire anodes for Lithium ion batteries, and comparison with the performance of other Si anode concepts, *Energies* 6 (10) (2013) 5145, doi:http://dx.doi.org/10.3390/en6105145.
- [18] S. Noehren, E. Quiroga-Gonzalez, J. Carstensen, H. Foell, Electrochemical Fabrication and Characterization of Silicon Microwire Anodes for Li Ion Batteries, *J. Electrochem. Soc.* 163 (6) (2016) A1, doi:http://dx.doi.org/10.1149/2.011603jes.
- [19] W.R. Liu, Z.Z. Guo, W.S. Young, D.T. Shieh, H.C. Wu, M.H. Yang, N.L. Wu, Effect of electrode structure on performance of Si anode in Li-ion batteries: Si particle size and conductive additive, *J. Power Sourc.* 140 (2005) 139, doi:http://dx.doi.org/10.1016/j.jpowsour.2004.07.032.
- [20] M. Cerbelaud, B. Lestriez, D. Guyomard, A. Videcoq, R. Ferrando, Brownian Dynamics Simulations of Colloidal Suspensions Containing Polymers as Precursors of Composite Electrodes for Lithium Batteries, *Langmuir* 28 (2012) 10713, doi:http://dx.doi.org/10.1021/la302135v.

- [21] M.N. Obrovac, V.L. Chevrier, Alloy Negative Electrodes for Li-Ion Batteries, *Chem. Rev.* 114 (2014) 11444, doi:<http://dx.doi.org/10.1021/cr500207g>.
- [22] T. Chen, L. Pan, X. Liu, Z. Sun, A comparative study on electrochemical performances of the electrodes with different nanocarbon conductive additives for lithium ion batteries, *Mater. Chem. and Phys.* 142 (2013) 345, doi:<http://dx.doi.org/10.1016/j.matchemphys.2013.07.027>.
- [23] L. Chen, X. Xie, J. Xie, K. Wang, J. Yang, Binder effect on cycling performance of silicon/carbon composite anodes for lithium ion batteries, *J. Appl. Electrochem.* 36 (2006) 1099, doi:<http://dx.doi.org/10.1007/s10800-006-9191-2>.
- [24] S.D. Beattie, D. Larcher, M. Morcrette, B. Simon, J.M. Tarascon, Si electrodes for Li-ion batteries—A new way to look at an old problem, *J. Electrochem. Soc.* 155 (2) (2008) A158, doi:<http://dx.doi.org/10.1149/1.2817828>.
- [25] A. Magasinski, B. Zdyrko, I. Kovalenko, B. Hertzberg, R. Burtovoy, C.F. Huebner, T. F. Fuller, I. Luzinov, G. Yushin, Towards efficient binders for Li-ion batteries Si-based anodes: Polyacrylic Acid, *ACS Appl. Mater. Interfaces* 2 (11) (2010) 3004, doi:<http://dx.doi.org/10.1021/am100871y>.
- [26] B. Lestriez, S. Bahri, I. Sandu, L. Roue, D. Guyomard, On the binding mechanism of CMC in Si negative electrodes for Li-ion batteries, *Electrochem. Comm.* 9 (2007) 2801, doi:<http://dx.doi.org/10.1016/j.elecom.2007.10.001>.
- [27] A. Etienne, A. Tranchot, T. Douillard, H. Idrissi, E. Maire, L. Roué, Evolution of the 3D Microstructure of a Si-Based Electrode for Li-Ion Batteries Investigated by FIB/SEM Tomography, *J. Electrochem. Soc.* 163 (2016) A1550, doi:<http://dx.doi.org/10.1149/2.0421608jes>.
- [28] C.C. Nguyen, T. Yoon, D.M. Seo, P. Guduru, B.L. Lucht, Systematic Investigation of Binders for Silicon Anodes: Interactions of Binder with Silicon Particles and Electrolytes and Effects of Binders on Solid Electrolyte Interphase Formation, *ACS Applied Materials & Interfaces* 8 (2016) 12211, doi:<http://dx.doi.org/10.1021/acsami.6b03357>.
- [29] R.G. Compton, C.E. Banks, *Understanding Voltammetry*, Imperial College Press, London, 2011.
- [30] J. Heinze, Cyclic voltammetry-electrochemical spectroscopy, *Angew. Chem. Int. Ed. Engl.* 23 (11) (1984) 831, doi:<http://dx.doi.org/10.1002/anie.198408313>.
- [31] E. Gileadi, *Physical Electrochemistry—Fundamentals, Techniques and Applications*, Wiley–VCH, Weinheim, 2011.
- [32] C.K. Chan, R. Ruffo, S.S. Hong, R.A. Huggins, Y. Cui, Structural and electrochemical study of the reaction of lithium with silicon nanowires, *J. Power Sources* 189 (2009) 34, doi:<http://dx.doi.org/10.1016/j.jpowsour.2008.12.047>.
- [33] K. Karki, E. Epstein, J.H. Cho, Z. Jia, T. Li, S.T. Picraux, C. Wang, J. Cumings, Lithium-Assisted Electrochemical Welding in Silicon Nanowire Battery Electrodes, *Nano Lett* 12 (3) (2012) 1392, doi:<http://dx.doi.org/10.1021/nl204063u>.
- [34] M. Pharr, K. Zhao, X. Wang, Z. Suo, J.J. Vlassak, Kinetics of Initial Lithiation of Crystalline Silicon Electrodes of Lithium-Ion Batteries, *Nano Lett* 12 (9) (2012) 5039, doi:<http://dx.doi.org/10.1021/nl302841y>.
- [35] H. Haftbaradaran, H. Gao, W.A. Curtin, A surface locking instability for atomic intercalation into a solid electrode, *Appl. Phys. Lett.* 96 (2010) 091909, doi:<http://dx.doi.org/10.1063/1.3330940>.
- [36] K. Zhao, M. Pharr, Q. Wan, W.L. Wang, E. Kaxiras, J.J. Vlassak, Z. Suo, Concurrent Reaction and Plasticity during Initial Lithiation of Crystalline Silicon in Lithium-Ion Batteries, *J. Electrochem. Soc.* 159 (3) (2012) A238, doi:<http://dx.doi.org/10.1149/2.020203jes>.
- [37] J. Wang, *Analytical Electrochemistry*, John Wiley & Sons, New Jersey, 2006.
- [38] D.R. Ferrier, R.R. Schroeder, Staircase voltammetry with varied current sampling times, *Electroanal. Chem. Interfac. Electrochem.* 45 (3) (1973) 343, doi:[http://dx.doi.org/10.1016/s0022-0728\(73\)80045-2](http://dx.doi.org/10.1016/s0022-0728(73)80045-2).
- [39] J. Newman, K.E. Thomas-Alyea, *Electrochemical Systems*, John Wiley, New Jersey, 2004.